The Isolated C-Terminal Domain of Ring1B Is a Dimer Made of Stable, Well-Structured Monomers †

ARTICLE *in* BIOCHEMISTRY · DECEMBER 2007

Impact Factor: 3.02 · DOI: 10.1021/bi701343q · Source: PubMed

8 AUTHORS, INCLUDING:

Francisco N. Barrera
University of Tennessee
44 PUBLICATIONS **655** CITATIONS
SEE PROFILE

Estefania Hurtado
Swedish Orphan Biovitrum
10 PUBLICATIONS **108** CITATIONS
SEE PROFILE

Miguel Vidal
Centro de Investigaciones Biológicas
66 PUBLICATIONS **6,668** CITATIONS
SEE PROFILE

The Isolated C-Terminal Domain of Ring1B Is a Dimer Made of Stable, Well-Structured Monomers†

Anna Czypionka,‡,# Olga Ruiz de los Paños,‡,⊗ Mauricio G. Mateu,§ Francisco N. Barrera,‡ Estefanía Hurtado-Gómez,‡ Javier Gómez,‡ Miguel Vidal,|| and José L. Neira‡,⊥,#,*

Instituto de Biología Molecular y Celular, Universidad Miguel Hernández, 03202 Elche (Alicante), Spain, Centro de Biología Molecular "Severo Ochoa" (CSIC-UAM), Universidad Autónoma de Madrid, 28049 Madrid, Spain, Centro de Investigaciones Biológicas, CSIC, 28040 Madrid, Spain, and Biocomputation and Complex Systems Physics Institute, 50009 Zaragoza, Spain

Received July 9, 2007; Revised Manuscript Received August 28, 2007

ABSTRACT: The Ring1B is a core subunit protein of the PRC1 (polycomb repressive complex 1), which plays key roles in the regulation of the *Homeobox* gene expression, X-chromosome inactivation, stem cell self-renewal, and tumorigenesis. The C-terminal region of Ring1B interacts with RYBP, a transcriptional repressor in transiently transfected cells, and also with M33, another transcriptional repressor involved in mesoderm patterning. In this work, we show that the C-terminal domain of Ring1B, C-Ring1B, is a dimer in solution, with a dissociation constant of 200 μM, as shown by NMR, ITC, and analytical gel filtration. Each monomer is stable at physiological conditions in a wide pH range ($\sim$5 kcal mol^{-1} at 298 K), with a well-formed core and a spherical shape. The dimer has a high content of α-helix and β-sheet, as indicated by FTIR spectra, and it is formed by the mutual docking of the preformed folded monomers. Since the C-terminal region is important for interaction with other proteins of the PRC1, the dimerization and the presence of those well-structured monomers might be a form of regulation.

Physiological processes involve a complex network of biochemical activities. The biological specificity and functional plasticity of such processes depend on their spatial and temporal coupling in cells. This coupling is provided by macromolecular assemblies, which are diverse in function, composition, and cellular location. Although the biochemical activities characterizing some biological functions are known, the physicochemical bases behind the macromolecular organization and assembly of complexes governing those activities still remain poorly understood (*1*).

The polycomb group proteins (PcG[1]) are a set of evolutionarily conserved, general transcriptional repressors, which are essential for maintaining the transcription pattern of key regulatory genes through development in many organisms (*2*, *3*). The PcG are best known as repressors of the *Hox* (homeobox) gene along the anterior−posterior animal body axis. Two major PcG complexes have been characterized in *Drosophila*: the Polycomb repressive complex (PRC1) and the ESC−E(Z) complex, also called PRC2 (*4*, *5*). The core subunits of both complexes are conserved in mammals (*6*), and both have been implicated in epigenetic inheritance, tumorigenesis, senescence, and cell development (*7*, *8*). The PRC2 is a histone methyltransferase complex able to methylate the histone H3 (*9*, *10*). On the other hand, the core complex of *Drosophila* PRC1 is formed by the polycomb, posterior sex combs, polyhomeotic and Ring finger proteins (*11*); those proteins block the nucleosome by generating a higher-order chromatin structure refractory to gene transcription. Furthermore, Ring domains are of great interest because of their widespread occurrence and diversity, since they have been involved in cell growth, apoptosis, antiviral response, ligase activity, and organelle biogenesis (*1*). For instance, it has recently been shown that a human PRC1, composed of several proteins, including Ring1A and Ring1B, is an E3 ubiquitin ligase complex that mono-ubiquitinates the nucleosomal histone H2A (*12*). This ligase activity is involved in X-chromosome inactivation and control of the *Hox* gene expression (*13*−*15*).

† This work was supported by grants CTQ2005-00360/BQU from the Spanish Ministerio de Educación y Ciencia (MEC) to J.L.N. and SAF2004-06952-C02-01 to M.V. Work at the Centro de Biología Molecular "Severo Ochoa" is supported by grant BIO2006-00793 from MEC to M.G.M. and an institutional grant from Fundación Ramón Areces. Estefanía Hurtado-Gómez was a recipient of a Ph.D. fellowship from Generalitat Valenciana. Francisco N. Barrera was a recipient of a Ph.D. fellowship from MEC.

* Corresponding author: José L. Neira, Instituto de Biología Molecular y Celular, Edificio Torregaitán, Universidad Miguel Hernández, Avda. del Ferrocarril s/n, 03202, Elche (Alicante), Spain. Tel: + 34 966658459. Fax: + 34 966658758. E-mail: jlneira@umh.es.

‡ Universidad Miguel Hernández.

§ Universidad Autónoma de Madrid.

|| CSIC.

⊥ Biocomputation and Complex Systems Physics Institute.

# These two authors contributed equally to this work.

⊗ Current address: Servicios Técnicos de Investigación, Universidad Miguel Hernández.

[1] Abbreviations: ANS, 8-anilinonapthalene-1-sulfonic acid; CD, circular dichroism; C-Ring1B, the C-terminal region of Ring1B (residues 227 to 334 of the intact protein); DOSY, diffusion-ordered spectroscopy; E3, ubiquitin-protein isopeptide ligase; FTIR, Fourier transform infrared; GdmCl, guanidine hydrochloride; $[GdmCl]_{1/2}$, concentration of GdmCl at the midpoint of the chemical-denaturation; ITC, isothermal titration calorimetry; NMR, nuclear magnetic resonance; PcG, polycomb group proteins; PRC1, Polycomb repressive complex 1; Ring, really interesting new gene; TSP, 3-(trimethylsilyl)-propionic acid-2,2,3,3-$^2H_4$-sodium salt; UV, ultraviolet.

10.1021/bi701343q CCC: $37.00
Published on Web 10/13/2007

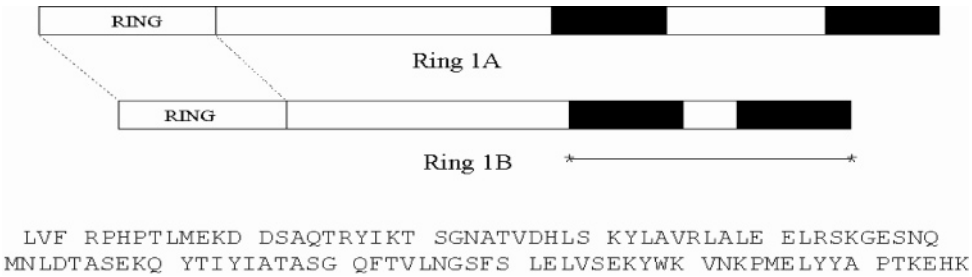

FIGURE 1: The organization of Ring1B: Domain organization of Ring1A and Ring1B proteins, indicating the conserved Ring domains; the conserved sequence regions in both proteins are shown in black. The sequence of C-Ring 1B (residues 227 to 334 of the intact protein) analyzed in this work is shown at the bottom, and the asterisks and the line through them indicate the position of such sequence in the intact protein.

In mouse, Ring1B is a 334-residues long protein that interacts with the repressor domain M33 (a murine homologue to the *Drosophila* Polycomb protein) (*16*) and RYBP (*17*), a second repressor protein. Ring1B has an N-terminal Ring finger motif; the protein shows a high sequence identity at the Ring region and at the C terminus of its paralog, Ring1A (Figure 1). The X-ray structure of the Ring domain of Ring1B when forming a complex with Bmi-1 (a homologue of the *Drosophila* posterior sex combs) has been solved (*18*). The Ring domain is composed of a three-stranded antiparallel β-sheet, two Zn^{2+} binding loops, and an α-helix following the second β-strand. Conversely, to date there is no structural information on the C-terminal region of Ring1B (Figure 1), which is the interacting region with M33 and RYBP (*16*, *17*), two repressor domains. Knowledge of the structure of this region would provide clues on the determinants of the interactions between PcG proteins and how these interactions can be regulated.

In this work, we describe the association and conformational preferences of the C terminal region of Ring1B, C-Ring1B. The isolated region is a low-affinity dimer with a dissociation constant of $\sim$200 μM, as shown by ITC, NMR, and analytical gel filtration chromatography. The isolated monomer of C-Ring1B is well-structured and contains a large amount of β-sheet and α-helix. Furthermore, the monomeric species is relatively stable ($\sim$5 kcal mol^{-1} at physiological conditions) in a wide pH range. Then it seems that intersubunit associations (within the dimer) or associations with other proteins are not important for the proper folding of the monomeric C-Ring1B; further, dimerization occurs by docking of the two preformed monomers. The dimer contains a high percentage of α-helix and β-sheet. We discuss the implications of both the low affinity dimerization constant and the stability of monomeric C-Ring1B in regulation of the binding to other proteins.

EXPERIMENTAL PROCEDURES

Materials. Urea and GdmCl ultrapure were from ICN Biochemicals. GdmCl molecular biology grade was from Sigma. Exact concentrations of urea and GdmCl were calculated from the refractive index of the solutions (*19*). Imidazole, Trizma base, NaCl, and ANS were from Sigma. β-Mercaptoethanol was from BioRad, and the Ni^{2+}-resin was from Invitrogen. Dialysis tubing with a molecular weight cutoff of 3500 Da was from Spectrapore. Standard suppliers were used for all other chemicals. Water was deionized and purified on a Millipore system.

Protein Expression and Purification. The C-Ring1B protein comprises residues 227−334 of the intact Ring1B and an additional His_6-tag at the N terminus, which does not contain any cleavage site. The tag was a kind gift from Dr. M. Bycroft and Mr. M. Proctor. Recombinant protein was expressed in *E. coli* C43 strain (*20*) and purified using Ni^{2+} chromatography. To eliminate any protein or DNA bound to the resin, coeluting with the protein, an additional gel filtration chromatography step was carried out by using a Superdex 75 16/60 gel filtration column (GE Healthcare). The final C-Ring1B yield was 30−35 mg of protein per liter of culture. The samples were dialyzed extensively against water, lyophilized, and stored at −80 °C. Protein concentration was calculated from the absorbance at 280 nm, using the extinction coefficients of model compounds (*21*). Samples for chemical-denaturation studies were prepared by dissolving the lyophilized protein either in deionized water (unfolding) or in 7 M GdmCl (folding). The domain contains seven tyrosine residues and one tryptophan (Figure 1).

NMR Spectroscopy. The NMR experiments were acquired on a Bruker Avance DRX-500 spectrometer equipped with a triple resonance probe and z-pulse field gradients.

(a) 1D-NMR Spectroscopy. Homonuclear 1D-NMR experiments were performed with sample concentrations ranging from 8 μM to 1.6 mM in 0.5 mL at 293 K, pH 7, 100 mM phosphate buffer (uncorrected for deuterium isotope effects) in H_2O/D_2O (90%/10%, v/v). TSP was used as the external chemical shift reference. 1D spectra were acquired with 16 K data points, averaged over 512 scans with 6000 Hz of spectral width (12 ppm); water suppression was achieved by WATERGATE (*22*). Baseline correction and zero-filling were applied. All spectra were processed and analyzed by using XWINNMR (Bruker GmbH, Karlsruhe, Germany) working on a PC computer.

(b) Translational Diffusion Measurements (DOSY experiments). Translational self-diffusion measurements were performed with the pulsed-gradient spin−echo NMR method in aqueous solution, where the viscosity can be easily obtained. The following relationship exists between the translational self-diffusion parameter, D, and the delays during acquisition (*23*, *24*):

$$\frac{I}{I_0} = -\exp\left(D\gamma_H{}^2\delta^2G^2\left(\Delta - \frac{\delta}{3} - \frac{\tau}{2}\right)\right) \qquad (1)$$

where I is the measured peak intensity of a particular (or a group of) resonance(s), I_0 is the maximum peak intensity of

the same resonance(s) at the smaller gradient strength, D is the translational self-diffusion constant (in $cm^2\ s^{-1}$); δ is the duration (in s) of the gradient, G is the strength of the gradient (in $T\ cm^{-1}$); Δ is the time (in seconds) between the gradients, γ_H is the gyromagnetic constant of the proton, and τ is the recovery delay between the bipolar gradients (100 μs). Data are plotted as the $-\ln(I/I_0)$ *versus* G^2 and the slope of the line is $D\gamma_H^2\delta^2(\Delta - \delta/3 - \tau/2)$, from where D can be easily obtained. The largest protein concentration used was 1.6 mM; the other concentrations were obtained from dilution of that stock. The duration of the gradient was varied between 2.2 and 3 ms, and the time between both gradients was changed between 100 and 150 ms. The most upfield shifted methyl groups (between -0.5 to 0.5 ppm) were used to measure the changes in intensity.

The Stokes−Einstein equation relates D to R, the hydrodynamic radius of a sphere, and the viscosity of the solvent, η, according to:

$$R = \frac{kT}{6\pi\eta D} \tag{2}$$

where T is the temperature (in K) and k the Boltzmann constant.

The viscosity of a solution is very weakly influenced by the macromolecule component in the μM range, and therefore the viscosity of the solution can be considered that of the solvent. Solvent viscosity is temperature-dependent (*25*): $\log \eta = a + [b/(c - T)]$. The terms a, b, and c are given for a particular D_2O:H_2O ratio. In our conditions, a 100% D_2O solution, the values were: $a = -4.2911$, $b = -164.97$ and $c = 174.24$. This yields a value of $\eta = 1.253$ kg/(cm s) at 293 K, used in our calculations.

The gradient strength was calibrated by using the diffusion rate for the residual proton water line in a sample containing 100% D_2O in a 5-mm tube, as described (*26*).

Gel Filtration Chromatography. The standards used in the column calibration and their corresponding Stokes radii were ribonuclease A (16.4 Å), chymotrypsinogen (20.9 Å), ovoalbumin (30.5 Å), and bovine serum albumin (35.5 Å) (*27*). Samples, in either procedure (see below), were loaded at 25 mM sodium phosphate, pH 7.3, in a calibrated Superdex 75 HR FPLC column (GE Healthcare), running on an FPLC system (GE Healthcare). Samples were eluted at 1 mL/min and continuously monitored with an on-line detector at a wavelength of 280 nm.

(*a) Analytical Gel Filtration Chromatography Used To Determine the* K_D. Association constants for the oligomerization equilibrium of C-Ring1B were determined as described (*28*). Two different procedures were followed. First, the association constant was determined by using gel filtration frontal elution (large zone) (*29*). Fifteen-milliliter aliquots of C-Ring1B samples with a total protein (monomer) concentration (C_t) ranging from 2 to 178 μM were loaded into the column. The elution volume, V_e, at each C_t was determined as the midpoint of the ascending frontal profile in the chromatogram. The weight average partition coefficient, σ, at each concentration of protein was calculated with:

$$\sigma = \frac{(V_e - V_t)}{(V_o - V_t)} \tag{3}$$

where V_o and V_t are the void and bed volumes of the column, with values of 8.13 ± 0.06 mL and 28.43 ± 0.03 mL, respectively. The V_o and V_t volumes were, respectively, determined using Blue dextran (5 mg/mL, in 10 mM phosphate buffer containing 150 mM NaCl) and L-tryptophan (0.5 mg/mL, in the same buffer) by averaging four measurements for each reagent. The experimental σ values obtained at the different C_t were fitted to (*28*):

$$\sigma = \sigma_m\left(\frac{-1 + \sqrt{1 + 8(1/K_D)C_t}}{4(1/K_D)C_t}\right) + \sigma_d\left(1 - \left(\frac{-1 + \sqrt{1 + 8(1/K_D)C_t}}{4(1/K_D)C_t}\right)\right) \tag{4}$$

where the σ_m and σ_d are the average partition coefficients of the monomer and dimer, respectively, and K_D is the dissociation constant.

Second, we also determined the dissociation constant by zonal elution (small zone) experiments. These elution experiments and calculation of the K_D were carried out in the same way as describe above, but 200-μL aliquots were loaded into the column. The elution volume was defined by the peak position in the chromatogram. This technique does not provide good estimates of the dissociation constant because of protein dilution effects in the column (*29*), but it allows exploration of higher protein concentrations, which would be prohibitive for large zone experiments. Thus, the concentrations explored in the small zone experiments were 5 to 1340 μM.

(*b) Analytical Gel Filtration Chromatography To Determine Hydrodynamic Parameters.* Gel filtration chromatography was also used to determine the R value of the monomeric and dimeric species, as described (*30*−*32*). In the experiments carried out at different pHs, the buffers (see below) were used at a final concentration of 50 mM with 150 mM of NaCl to avoid interactions with the column. Two protein concentrations were used: 10 and 50 μM.

Isothermal Titration Calorimetry (ITC) and Calculation of the K_D. The ITC experiments were carried out by using an Omega instrument (MicroCal Inc.) coupled to an external nanovoltmeter, which was used to improve the signal-to-noise ratio (*33*). Prior to the calorimetric experiments, the protein was concentrated and dialyzed at 278 K against the working buffer. In order to eliminate any trace of cations that might bind to the histidine-tag of the protein and interfere with the dissociation reaction, the syringe and the calorimetric cell were previously treated with a concentrated solution of EDTA. Dilution ITC experiments involved sequential injections of microliter amounts (20 μL) of concentrated protein solution (300 μM) into the calorimetric cell (1.4 mL), which initially contained buffer alone. The dilution of the protein solution shifts the equilibrium toward the monomer, and the amount of heat either released or absorbed upon dissociation into monomers can be monitored as a function of the total concentration of the protein in the calorimetric cell. Thus, in an ITC dilution experiment we measure the heat evolved, q, when a small volume of concentrated protein solution in the syringe, $[P]_{syr}$, is injected into the calorimetric cell. For the ith injection of a series, the observed heat, q_i, is given by the product of the dissociation enthalpy, ΔH_D, and the

number of moles of the protein that actually dissociate. This protein dissociation is a consequence of the drastic change of concentration, induced by the dilution of the protein from its initial concentration in the syringe, $[P]_{syr}$, to its final concentration in the calorimetric cell, $[P]_{cell}$:

$$q_i = n_{(P_2 \rightarrow 2P)} \Delta H_D$$

where the number of moles of protein changing their oligomeric state upon dilution depends on (i) the initial and final concentration of the protein ($[P]_{syr}$ and $[P]_{cell}$, respectively), and (ii) the dissociation constant, K_D.

The amount of power required to maintain the reaction cell at constant temperature after each injection was monitored as a function of time. The integration of each calorimetric peak (corrected for the appropriate buffer mixing control experiments) yields the apparent enthalpy change for protein dissociation. The concentration dependence of the apparent enthalpy change is, then related to K_D.

The thermodynamical parameters describing the dimer/monomer equilibrium were obtained by fitting the experimental data (apparent enthalpies of dissociation *versus* total protein concentration in the calorimetric cell) using the software package Origin 7.0 from MicroCal. The fitting procedure can be summarized as follows. If there are only two states available for the protein (namely, monomer, P, and dimer P_2), according to the mass action law we can express the K_D as:

$$P_2 \rightleftarrows P + P, \qquad K_D = [P]^2/[P_2] \tag{5}$$

The concentration of free monomer, [P], is obtained as a function of K_D, and the total concentration of the protein in the calorimetric cell, $[P]_{total}$:

$$[P] = \frac{(-K_D + \sqrt{K_D{}^2 + 8K_D[P]_{total}})}{4} \tag{6}$$

Equations 5 to 6 are used in standard nonlinear least-squares regression analysis to fit the experimental dilution data (apparent ΔH_D versus $[P]_{cell}$) to obtain K_D and ΔH_D.

Fluorescence Measurements. All fluorescence spectra were collected on a Cary Varian spectrofluorimeter, interfaced with a Peltier, at 298 K. Sample concentration in the pH-denaturation experiments was 1 μM; otherwise, it was 5 μM, and the final concentration of the buffer was, in all cases, 10 mM. A 1-cm path length quartz cell (Hellma) was used.

(*a) Steady-State Fluorescence Measurements.* The protein samples were excited at 280 and at 295 nm in the pH range 2−12 to characterize a possible different behavior of tryptophan or tyrosine residues (*34*). Chemical-denaturation experiments were acquired by excitation at 280 nm, because no differences were observed between the excitation either at 280 nm or at 295 nm (data not shown). The slit widths were typically equal to 5 nm for the excitation and emission light. The fluorescence experiments were recorded between 300 and 400 nm. The signal was acquired for 1 s and the increment of wavelength was set to 1 nm. Blank corrections were made in all spectra.

The chemical-denaturations, either followed by fluorescence or CD, were carried out by dilution of the proper amount of the 7 M GdmCl stock solution and leaving the samples overnight at 298 K. In the pH-induced unfolding experiments, the pH was measured after completion of the experiments, and essentially no differences were observed with those pHs calculated from the buffer stock solutions. The pH was measured with an ultrathin Aldrich electrode in a Radiometer (Copenhagen) pH-meter. The pH range explored was 2 to 12. The salts and acids used were as follows: pH 2.0−3.0, phosphoric acid; pH 3.0−4.0, formic acid; pH 4.0−5.5, acetic acid; pH 6.0−7.0, NaH_2PO_4; pH 7.5−9.0, Tris acid; pH 9.5−11.0, Na_2CO_3; pH 11.5−13.0, Na_3PO_4.

(b) ANS Binding. Excitation wavelength was 380 nm, and emission was measured from 400 to 600 nm. Slit widths were 5 nm for excitation and emission. Stock solutions of ANS were prepared in water and diluted into the samples to yield a final concentration of 100 μM. In all cases, blank solutions were subtracted from the corresponding spectra.

Circular Dichroism Measurements. Circular dichroism spectra were collected on a Jasco J810 spectropolarimeter fitted with a thermostated cell holder and interfaced with a Neslab RTE-111 water bath. The instrument was periodically calibrated with (+) 10-camphorsulphonic acid.

(a) Steady-State Spectra. Isothermal wavelength spectra at different pHs were acquired at a scan speed of 50 nm/min with a response time of 2 s and averaged over four scans at 298 K. Far-UV measurements were performed with 10 μM of protein in 10 mM buffer, in a 0.1-cm path length cells.

In the chemical-denaturation experiments, far-UV CD spectra were acquired at a scan speed of 50 nm/min, and four scans were recorded and averaged at 298 K. The response time was 4 s. The path length cell was 0.1 cm, with protein concentrations of 5.03, 15.1, and 30.2 μM. Spectra were corrected by subtracting the baseline in all cases. Every chemical denaturation experiment was repeated at least three times with new samples.

(b) Thermal Denaturation Experiments. Thermal denaturation experiments were performed at constant heating rates of 60 K/h and a response time of 8 s. Thermal scans were collected in the far-UV region at 222 nm from 298 to 363 K in 0.1-cm path length cells with a total protein concentration of 10 μM. The solution conditions were the same as those reported in the steady-state experiments. Heating led to precipitation in all cases. The possibility of drifting of the CD spectropolarimeter was tested by running two samples containing buffer, before and after the thermal experiments. No difference was observed between the scans.

Analysis of the pH- and Chemical-Denaturation Curves, and Free Energy Determination. The wavelength averaged emission intensity, $\langle\lambda\rangle$, in fluorescence spectra was calculated as described (*35*). The pH-denaturation experiments were analyzed assuming that both species, protonated and deprotonated, contributed to the fluorescence spectrum:

$$X = \frac{(X_a + X_b 10^{n(pH - pK_a)})}{(1 + 10^{n(pH - pK_a)})} \tag{7}$$

where X is the physical property being observed (ellipticity or fluorescence), X_a is the physical property being observed for the acidic species, X_b is the physical property observed at high pHs, pK_a is the apparent pK of the titrating group,

and n is the Hill coefficient (which was close to 1 in all the curves reported in this work). The apparent pK_a reported was obtained from three different measurements, prepared with new samples.

To facilitate comparison among the different biophysical techniques, data were converted to the fraction of folded molecules according to the expression:

$$f_N = \frac{(X - X_D)}{(X_N - X_D)} \quad (8)$$

where $X_N = \alpha_N + \beta_N[D]$ and $X_D = \alpha_D + \beta_D[D]$ are the corresponding fractions of the folded and unfolded states, respectively, for which a linear relationship with denaturant is assumed. The denaturation data were fitted to the two-state equation:

$$X = (X_N + X_D e^{(-\Delta G/RT)})/(1 + e^{(-\Delta G/RT)}) \quad (9)$$

where R is the gas constant, ΔG is the free energy of denaturation, and T is the temperature in K.

Chemical-denaturation curves at the different pHs were analyzed using a two-state unfolding mechanism, according to the linear extrapolation model: $\Delta G = m([D]_{1/2} - [D])$ (*19*), where [D] is the denaturant concentration, m is the slope of the line, and $[D]_{1/2}$ is that at the midpoint of the transition. Fitting by nonlinear least-squares analysis to eqs 7 and 9 was carried out by using the general curve fit option of Kaleidagraph (Abelbeck software) on a PC computer.

Fourier Transform Infrared Experiments. Samples of C-Ring1B in phosphate buffer 50 mM, pH 7, were dried in a Speed Vac concentrator (Savant, Farmingdale, NY), and resuspended in a final volume of 22 μL of D_2O. After 90 min, the H−D exchange of the protein was complete, as indicated by the fact that the absorbance at 1550 cm^{-1} did not further decrease. The samples were placed amid a pair of CaF_2 windows separated by a 50 μm thick Mylar spacer in a Harrick (Ossining, NY) demountable cell.

Experiments were performed with C-Ring1B at 0.5 and 1 mM, yielding similar results (data not shown). Spectra were acquired on a Nicolet 520 instrument equipped with a deuterated triglycine sulfate detector and fitted with a water bath. The cell container was continuously filled with dry air. Usually, 600 scans/sample were taken, averaged, apodized with a Happ-Genzel function, and Fourier transformed to give a final resolution of 2 cm^{-1}. The contributions of the buffer spectra were subtracted, and the resulting spectra were used for analysis, as described (*32*). The error in estimation of the percentage of secondary structure depends mainly on the removal of spectral noise, which was estimated to be 2% (*36*).

RESULTS

C-Ring1B is a Dimer with a Low Affinity Constant. We used three techniques, namely, NMR spectroscopy, analytical gel filtration chromatography, and ITC, which provided independent evidence of the presence of a monomer−dimer equilibrium in C-Ring1B. All three techniques yielded a very similar value for the association constant.

(a) NMR Measurements. We carried out diffusion measurements (DOSY-NMR) on C-Ring1B based on the following argument. If the oligomerization state of C-Ring1B changed upon protein concentration, the diffusion coefficient should change not only as a consequence of protein dilution (the translational diffusion coefficient of a protein, either monomeric or oligomeric, increases linearly as the protein concentration decreases, since at lower protein concentrations, the molecular impairment of the translational diffusion is smaller) but also because of the presence of an oligomerization equilibrium. Then we should expect two or more straight lines (depending on the number of equilibria) to intersect at particular concentration(s); these particular concentration(s) would yield the dissociation constant(s) of the oligomerization equilibrium(a). In the C-Ring1B concentration range explored (8 μM to 1.5 mM), we observed two straight lines, which intersected at 224 ± 30 μM (Figure 2 A). This *sole* intersection point indicates that C-Ring1B was affected by a *single* protein-concentration-dependent equilibrium.

We can further elaborate on these results, by trying to determine the exact size of the protein species present. The y-axis intersection of the straight-line at low protein concentrations was 8.6 (±0.1) × 10^{-7} cm^2 s^{-1} (Figure 2A), which is the translational diffusion coefficient at infinite dilution; then the hydrodynamic radius, R, for a spherical C-Ring1B species is 19.9 ± 0.4 Å (eq 2). The R value for an ideal unsolvated spherical molecule can be theoretically calculated by considering that the anhydrous molecular volume, $M\bar{V}/N$, equals the volume of a sphere (*37*, *38*), R, and thus $R = \sqrt[3]{3M\bar{V}/4N\pi}$, where M is the molecular mass of the protein, $\bar{V}$ is its partial specific volume, and N is the Avogadro's number. The molecular mass of the monomeric histidine-tagged C-Ring1B is 13561.13 Da, and $\bar{V} = 0.71$ cm^3/g as calculated from amino acid composition (*38*) (Figure 1). The R value is 15.6 Å, but since the hydration shell is 3.2 Å wide (*39*), the hydration radius is 18.8 Å which is similar to that obtained from diffusion measurements (19.9 ± 0.4 Å). Then this low-concentration straight-line corresponds to the monomer of C-Ring1B (which, based on the agreement between both values of R, would be spherical). Thus, the high-concentration straight-line must involve an equilibrium with the monomeric species of C-Ring1B.

We also tried to find out the molecularity of the oligomeric species, by using the high-concentration straight-line. The y-axis intersection of this line is 7.4 (±0.1) × 10^{-7} cm^2 s^{-1}, which yielded an R value for a spherical C-Ring1B species of 22.8 ± 0.2 Å (eq 2). The theoretical radius for an unsolvated spherical dimeric C-Ring1B is 19.6 Å (determined from the above equations), and then the hydration radius is 22.8 Å, which is identical to that obtained from the translational diffusion coefficients. Then we suggest that (i) the high-concentration straight-line corresponds to a dimeric species, and (ii) C-Ring1B was involved in a monomer−dimer equilibrium, with a dissociation constant of 224 ± 30 μM.

(b) Analytical Gel Filtration Chromatography. Since C-Ring1B was involved in a monomer−dimer equilibrium, we fitted the experimental data obtained by analytical gel filtration, using either frontal or zonal elution, to eq 4. The experimental data fitted well to a second-order process, as expected. The K_D was similar in both procedures and identical, within the experimental error, to that determined

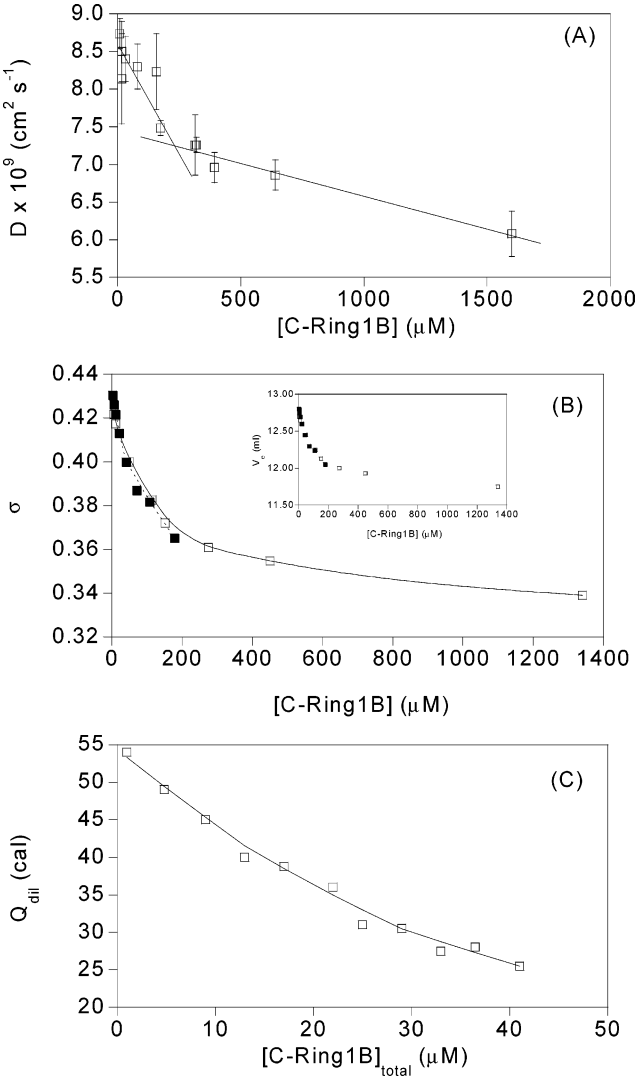

FIGURE 2: Association constant of C-Ring1B: (A) NMR diffusion coefficients of C-Ring1B as a function of protein concentration. The bars are fitting errors to eq 1. The solid lines are the fittings to linear equations whose *y*-axis intersections yield the diffusion coefficient at 0 M protein concentration for the dominant low- and high-protein concentration species. The low-protein concentration line was D (cm^2 s^{-1}) = 8.58 (±0.15) − 0.006 (±0.001) C_t. The high-concentration line was D (cm^2 s^{-1}) = 7.45 (±0.08) − 0.0008 (±0.0001) C_t. Conditions: 293 K, in phosphate buffer (pH 7), 50 mM. (B) Changes in σ as the concentration of monomeric protein was increased: blank squares (zonal elution) and filled squares (frontal elution). The fitting values for the frontal elution were: σ_m = 0.432 ± 0.002, and σ_d = 0.29 ± 0.01, and those for the zonal elution: σ_m = 0.428 ± 0.002, and σ_d = 0.308 ± 0.005. Inset: Changes in elution volume (mL) as the concentration of monomeric protein was increased (zonal elution). Conditions: 298 K, in phosphate buffer (pH 7), 50 mM with 150 mM NaCl. Data were fitted to eq 4. (C) Heat titration curve of C-Ring1B determined by using a VP−ITC at 298 K. Concentration of C-Ring1B was 0.3 mM (measured in units of monomeric protein) in the syringe, and each injection contained a volume of 20 μL, in 50 mM phosphate buffer (pH 7). Data were fitted to eqs 5 and 6.

by translational diffusion measurements. The frontal elution procedure yielded a K_D of 211 ± 47 μM, and the zonal elution procedure yielded a value of 218 ± 32 μM (Figure 2B).

(c) ITC Experiments. The dissociation of the dimeric form of C-Ring1B was induced upon dilution of a concentrated solution of the protein (above the previously K_D determined by the other techniques) into the calorimetric cell containing

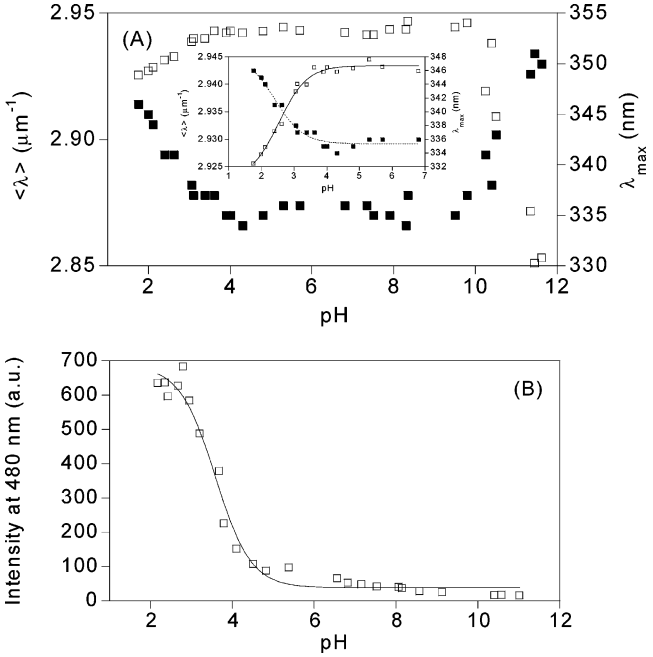

FIGURE 3: pH-induced structural changes of the monomeric species of C-Ring1B followed by fluorescence: (A) Intrinsic fluorescence: The $\langle\lambda\rangle$ (blank squares) and the maximum wavelength (filled squares) obtained by excitation at 280 nm are represented *versus* the pH. Inset: Expanded plot of the low-pH region, showing the fitting to eq 7. (B) Changes in the fluorescence intensity of ANS at 480 nm. Protein concentration was 1 μM (measured in units of monomeric protein); ANS concentration was 100 μM; buffer concentration was 10 mM in all cases. The line through the data is the fitting to eq 7.

the buffer. The dissociation of the dimer was shown to be endothermic (ΔH = 15.1 ± 5 kcal mol^{-1}), with a K_D of 195 ± 80 μM (at 298 K) (Figure 2C). Although the explored protein concentration range in the ITC measurements was 5-fold lower than the determined K_D (40 μM versus 195 μM) (Figure 2C), the fact that there is an agreement among the determined dissociation constants from the different experimental biophysical techniques make us feel confident that the measured value from ITC, even with such large error, is real.

To sum up, from these results with three different techniques, we can conclude that C-Ring1B is a dimer with a dissociation constant of ∼ 200 μM.

The Structure and pH-Induced Conformational Changes of Monomeric C-Ring1B. To characterize the structure and the stability of the monomeric species, we used intrinsic and ANS fluorescence, CD, and gel filtration chromatography.

(a) Steady-State Fluorescence Spectroscopy. We used fluorescence to monitor changes in the tertiary structure of the protein, around the single tryptophan and the seven tyrosines (Figure 1), as the pH was modified (*34*). The emission fluorescence spectrum of C-Ring1B at concentrations of 1 μM (where the percentage of dimer should be 0.5%) had a maximum at 335 nm at neutral pH, and then it was dominated by the emission of the sole tryptophan residue. From the blue-shifted maxima, we can conclude that the tryptophan is completely buried in the structure. As the pH varied, the maxima wavelengths of the spectra were red-shifted toward 350 nm, probably because of basic or acidic unfolding (Figure 3A, filled squares).

We examined the fluorescence spectra obtained by excitation at 280 and 295 nm, by using the $\langle\lambda\rangle$ (Figure 3A, blank squares). The tendency in the fluorescence spectra obtained when excitation was carried out at 295 nm was similar to that observed at 280 nm (data not shown). The profile of $\langle\lambda\rangle$ upon excitation at 280 nm *versus* pH showed two titrations at low and high pH. We could not determine reliably the pK_a of the titration at high pH (data not shown), which is related with the deprotonation of some, if not all, of the tyrosine, arginine, or lysine residues (*37*). On the other hand, the apparent pK_a of the titration at low pH was 2.5 ± 0.5 (determined by using eq 7 from pH 2 to 7, Figure 3A, inset). A similar value was obtained (2.4 ± 0.3) when the changes in the maxima wavelengths were followed. This pK_a was smaller than that of the side-chains of solvent-exposed Glu (4.25 ± 0.05), Asp (3.67 ± 0.04), and/or C-terminal residues (3.67 ± 0.03) (*40*), suggesting that the residues involved are probably deeply buried in the C-Ring1B structure.

(b) ANS Binding. ANS binding was used to monitor the extent of exposure of protein hydrophobic regions and to detect the existence of non-native partially folded conformations (*41*). At low pH, the fluorescence intensity at 480 nm was large and decreased as the pH was raised (Figure 3B), suggesting that at low pH the protein is exposing hydrophobic regions. The intensity at 480 nm showed a sigmoidal behavior with a pK_a = 3.4 ± 0.5, which is similar within the error to that determined by intrinsic fluorescence (Figure 3A inset). The difference between both values cannot be easily rationalized at this stage, but the most plausible explanation could be that different acidic residues are monitoring the acquisition of tertiary structure (intrinsic fluorescence) and the burial of hydrophobic regions (ANS fluorescence).

(c) Far-UV CD Experiments. We used far-UV CD as a spectroscopic probe that is sensitive to protein secondary structure (*42*, *43*). Because of the intrinsic sensitivity of the technique, the experiments were carried out at 10 μM of protein concentration (where the percentage of dimeric species would be lower than 1%). The CD spectrum of monomeric C-Ring 1B was very intense and had the features of an α-helical protein (Figure 4A, inset). This shape was not altered in a wide pH range (between pH 4 and 8.5), but at extreme pH values, the shape and the ellipticity at 222 nm changed (Figure 4A), suggesting that the secondary structure was altered; the changes were, however, small, since the total change of ellipticity was smaller than 1 mdeg. The tendency in the ellipticity at 222 nm was similar to that observed by fluorescence (see above): the ellipticity remained constant in a wide pH range and increased (in absolute value) at the extremes of pH (Figure 4A).

We have also tried to determine the midpoint of the transition observed at acidic pH in CD (Figure 4A, left side); the value (3.8 ± 1.2) was closer to that observed by ANS experiments (see above). However, the scattering of data at the acidic baseline yielded a large error, and thus it precluded its further use.

(*d) Gel Filtration Experiments.* Since the elution volume of C-Ring1B was concentration-dependent (see above), we carried out gel filtration experiments at different pHs at low (10 μM) and high protein concentrations (50 μM, where the percentage of dimeric species would be about 10%). Between

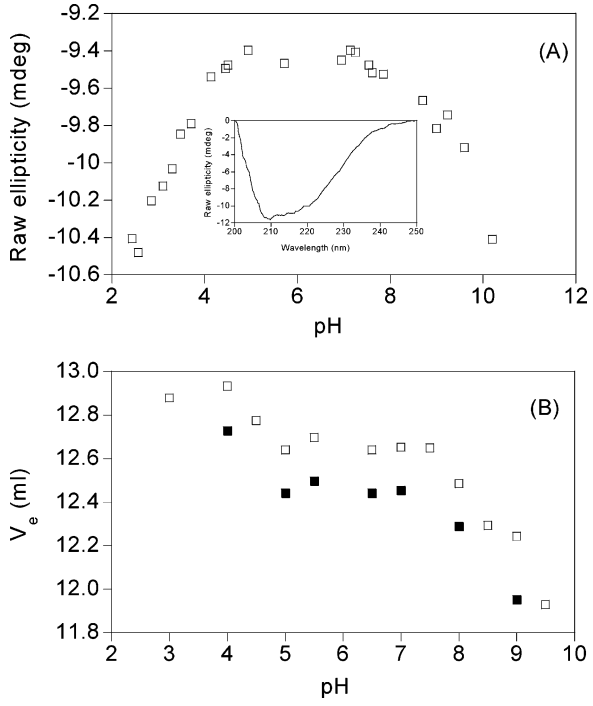

FIGURE 4: pH-induced structural changes of the monomeric species of C-Ring1B followed by CD and gel filtration: (A) Changes in the ellipticity at 222 nm in the far-UV CD spectra upon pH. Inset: Far-UV CD spectra at pH 7. Protein concentration was 10 μM; buffer concentration was 10 mM in all cases; the spectra were acquired in 0.1-cm path length cells. (B) The elution volumes a protein concentration (measured in units of monomeric protein) of 10 μM (blank squares) and 50 μM (filled squares) are shown. The concentration of the corresponding buffer at each pH was 50 mM plus 150 mM NaCl to avoid interactions with the column.

pH 5 and 7, the elution volume of the protein was constant (at ~12.70 mL). At high pH, the elution volume was smaller (Figure 4B), suggesting that (i) the protein had changed its shape, (ii) an aggregated species was present, or (iii) the value of K_D was pH-dependent. Conversely, at acidic pH the elution volume was larger, suggesting, based on the results from ANS binding, fluorescence, and CD, that the protein showed interactions with the column, probably due to the exposure of hydrophobic regions. Alternatively, this behavior at low pH could also be explained as due to changes in the dissociation constant. The tendency in the elution volume as the pH varied (except at acidic pH) was similar to that observed by intrinsic and ANS fluorescence (Figure 3) and CD (Figure 4A). There were, however, subtle differences, since in gel filtration experiments, the changes at basic pH occurred around pH 7 (Figure 4B), as in CD (Figure 4A), compared with the changes observed by fluorescence (Figure 3A), which occurred around pH 8. These findings might be due to two different reasons: first, that the K_D could be pH-dependent; and, second that the protein compactness was lost at lower pH than the tertiary structure around the sole tryptophan.

We can use the elution volume of the monomeric species to determine the hydrodynamic radius of the protein, according to the equations developed by Ackers and coworkers (*30*, *31*). The calculated *R* value was 19.4 ± 0.5 Å, which agrees very well with that determined previously by DOSY experiments (19.9 ± 0.4 Å).

Results at 50 μM showed a similar tendency than at the lower protein concentration (Figure 4B, filled squares). Then

the pH-related changes in the elution volume were not associated with a larger population of dimeric species but with the intrinsic behavior of the monomeric ones.

In conclusion, all spectroscopic probes indicate that monomeric C-Ring1B maintained its secondary and tertiary structure and a spherical shape within a wide pH range, between pH 4 and 7 (the latter value obtained from CD and gel filtration experiments, Figure 4B). Evidence of basic unfolding is observed in the fluorescence (tertiary structure), CD (secondary and, possibly, tertiary structure), and gel filtration experiments (compactness). On the other hand, at low pH, the losses of tertiary (fluorescence) and secondary structures (CD) are accompanied by an exposure of hydrophobic patches (ANS binding), which probably causes nonspecific interactions with the column.

The Stability of Monomeric C-Ring1B. We first carried out thermal denaturation experiments by using far-UV CD to obtain the thermodynamical parameters characterizing the unfolding transition of C-Ring1B.

(a) Thermal Denaturation Experiments by Far-UV CD. We explored the thermal-denaturation of C-Ring1B in the 2.5−11.5 pH range. The thermal profiles showed a sigmoidal behavior between pH 5 to 9 (Figure 1A, Supporting Information). At pH below 4, the thermal denaturations did not show a sigmoidal behavior (Figure 1B, Supporting Information). However, in all cases, the transitions were irreversible, precluding further thermodynamic analysis of the data. Irreversibility was also observed in the presence of different amounts of GdmCl (data not shown).

(b) Chemical-Denaturation Experiments. Since no thermodynamical information could be obtained from thermal denaturation measurements, we tried to determine the stability of C-Ring1B by using chemical reagents. We first carried out chemical-denaturations in the presence of urea; however, the unfolding baseline did not contain enough points, precluding a reliable determination of any thermodynamical parameter (data not shown). Then we chose GdmCl as the denaturant. We tested the reversibility of the chemical-denaturations by measuring the superposition of the sigmoidal curves obtained by fluorescence, starting from the fully folded (unfolding) or the fully denatured (folding) protein. The chemical-denaturation of C-Ring1B was reversible as shown by the agreement of the thermodynamic parameters at pH 7.0: the $[GdmCl]_{1/2}$ was 2.02 ± 0.02 M, *versus* 1.94 ± 0.06 M, when starting from fully folded protein, and the *m* values were 2.6 ± 0.5 kcal $mol^{-1}M^{-1}$ (fully unfolded protein) *versus* 2.6 ± 0.4 kcal mol^{-1} M^{-1} (from fully folded protein) (data not shown). Reversibility was also tested at pH 5.0 and 9.7 (data not shown).

(1) Fluorescence Measurements. We carried out chemical-denaturations at different pHs, to test whether the stability, as it happens with the conformational propensities (see above), did not change within a wide pH range. At all the explored pHs, the maxima wavelengths of the fluorescence spectra were red-shifted and the intensity decreased as the [GdmCl] increased. At pH 7, a single transition was observed (Figure 5A), which within the explored concentration range (1−50 μM), showed the same midpoint (Table 1). Since a monomer−dimer equilibrium is present in C-Ring1B, we could be tempted to conclude that the single chemical transition observed by fluorescence must involve the concomitant dissociation of the dimeric species and unfolding

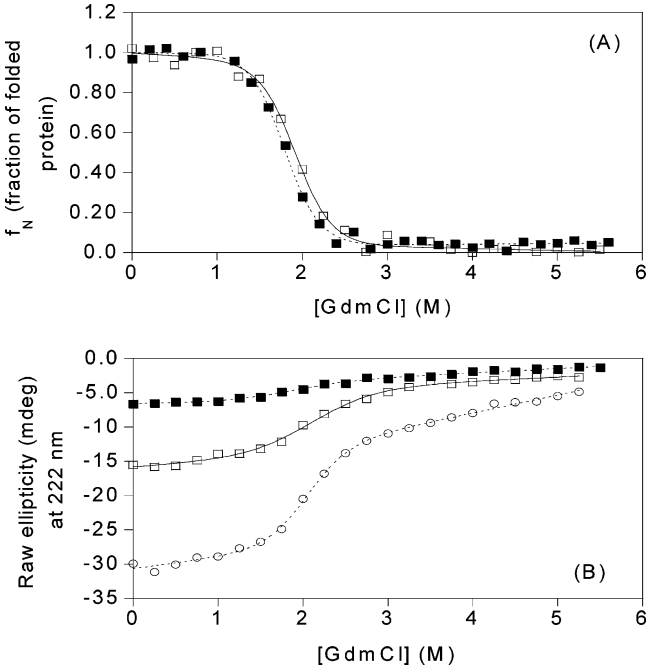

FIGURE 5: Chemical-denaturation of C-Ring1B followed by different biophysical techniques: (A) The normalized fluorescence data ($\langle\lambda\rangle$) at 5 μM of protein concentration (filled squares) and the normalized CD data (230 nm) at 15.1 μM of protein concentration (blank squares). (B) The raw ellipticity data at 222 nm obtained for 5.03 (filled squares), 15.1 (blank squares), and 30.2 μM (blank circles) of monomer concentration; similar sigmoidal curves were obtained by following the ellipticity at 230 nm, as shown by the normalized data at 15.1 μM in A. The lines through the data are the fittings to eq 9, by using the lineal extrapolation model.

of the resulting monomeric species. However, as the $[GdmCl]_{1/2}$ was not altered in a wide concentration range, the observed transition must monitor an unimolecular process and not a dissociation (bimolecular) step. The reasons behind this spectroscopic blindness will be described in the Discussion.

The free energy, as well as other thermodynamic parameters at different pHs, determined by fluorescence, are shown in Figure 6. C-Ring1B was moderately stable at acidic and neutral pH. Its maximum conformational stability at 298 K was 5.2 ± 0.4 kcal mol^{-1} (the average of the unfolding free energy values measured between pH 6 and 8.5), and occurred over a broad pH interval. This indicates that the interval where the conformational stability remained constant (from pH 6 to 8.5) was different from that observed in the structural changes monitored by the spectroscopic techniques (from pH 4 to 7.0; see above**)**. Probably, as it happens in other proteins (*44*), the measurement of the stability is a more sensitive probe to monitor small conformational changes rather than the amount of native-like secondary and tertiary structures. The *m* values were fairly constant over the pH range explored (Figure 6B), with an average value of 2.7 ± 0.2 kcal $mol^{-1}M^{-1}$.

(2) CD Measurements. Experiments were carried out at 5.03 μM protein concentration, at pH 7.0, where a single sigmoidal transition was also observed (Figure 5A). The $[GdmCl]_{50\%}$ was: 1.9 ± 0.1 M, and the *m* value was 2.2 ± 0.6 kcal mol^{-1} M^{-1} (at 230 nm); and 1.8 ± 0.2 M, and 1.6 ± 0.4 kcal mol^{-1} M^{-1} for the $[GdmCl]_{1/2}$ and the *m* values at 222 nm, respectively. The large errors are due to the small concentration used in the experiments. The *m* and $[GdmCl]_{1/2}$

Table 1: Thermodynamic Parameters of C-Ring1B Obtained by Chemical-Denaturation Experiments[a]

biophysical probe	[C-Ring1B] (μM)[b]	ΔG^0 (kcal mol^{-1})	m (kcal mol^{-1} M^{-1})	$[GdmCl]_{1/2}$ (M)
fluorescence	5	4.9 ± 0.5	2.6 ± 0.2	1.95 ± 0.06
	35	5.2 ± 0.6	2.8 ± 0.3	1.86 ± 0.03
	60	4.9 ± 0.6	2.7 ± 0.3	1.82 ± 0.05
CD[c]	5.03	4.1 ± 0.6	2.3 ± 0.6	1.8 ± 0.2
	15.1	4.1 ± 0.4	2.1 ± 0.2	1.92 ± 0.04
	30.2	4.8 ± 0.7	2.4 ± 0.3	2.01 ± 0.04

[a] ΔG^0 is the free energy of unfolding extrapolated to the absence of denaturant; m is the variation in the free energy of unfolding with the denaturant concentration. Errors in the m- and $[GdmCl]_{1/2}$ values are fitting errors. The uncertainty in ΔG^0 was obtained from error propagation, assuming that the errors in the m- and $[GdmCl]_{1/2}$ values are independent. Repetitions of the chemical denaturation experiments yielded differences of 0.2 kcal mol^{-1} M^{-1} in the m values, and of 0.02 M in the $[GdmCl]_{1/2}$. All experiments were carried out at 298 K. [b] The values of the concentration of C-Ring1B refer to the total protein concentration of monomer. [c] The values shown here are those obtained by following the changes in the ellipticity at 222 nm; similar values were observed by following the changes at 230 nm (data not shown).

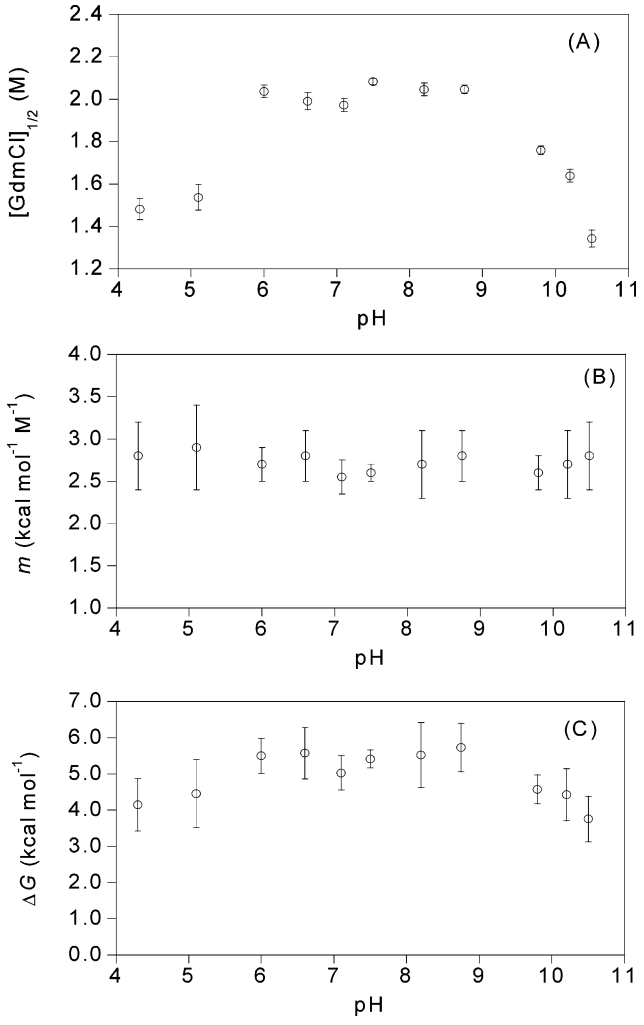

FIGURE 6: Stability of monomeric C-Ring1B at different pHs monitored by fluorescence, in chemical-denaturation experiments: (A) The midpoints of the denaturation curves. (B) The m values. The midpoint and the m values were obtained by using eq 9 and the lineal extrapolation model. (C) Curve of stability with the pH of C-Ring1B at 298 K. The free energy was obtained by the product of the m and $[GdmCl]_{1/2}$ values at the corresponding pH. Conditions: 5 μM of protein (expressed in units of monomeric protein); buffer concentration was 10 mM in all cases. Spectra were acquired in 1-cm path length cells.

values, and then the ΔG, were similar, within the experimental uncertainty, to those measured by fluorescence (Table 1). Furthermore, denaturation experiments carried out at higher protein concentrations (15.1 μM and 30.2 μM, where the percentage of the dimeric protein would be 1.75 μM and 5.8 μM, respectively) showed the same midpoint as at low concentration (at both wavelengths, 222 and 230 nm) (Table 1, Figure 5B). Interestingly, the native baseline of the CD experiments showed a larger slope as the concentration of protein increased: at 230 nm, it varied from 0.38 (5 μM), 0.46 (15.09 μM) to 1.07 (30.18 μM); at 222 nm, it went from 0.21 (5 μM), 0.57 (15.09 μM) to 1.65 (30.18 μM). These data suggest that probably, because of the small population of dimeric species, dissociation might be occurring at low [GdmCl], and it might be obscured by the native baseline. In conclusion, monomeric C-Ring1B was well-folded with a spherical shape, and a free energy of 5.2 ± 0.4 kcal mol^{-1}.

The Structure and Shape of Dimeric C-Ring1B. The 2D-NMR experiments of the dimeric C-Ring1B (at ~1 mM protein concentration) yielded poor TOCSY spectra, and NOESY experiments showed peak broadening. We could not carry out the spectroscopic characterization with most of the used techniques in monomeric C-Ring1B because of (i) the prohibitive large amounts of protein necessary to significantly populate the dimeric species (at a percentage larger than 80%), and/or (ii) signal saturation in some of the techniques. Thus, only structural studies with the dimeric species of C-Ring1B were carried out at pH 7 by using FTIR. Gel filtration analysis also provided some clues on the protein shape at physiological pH.

(a) Gel Filtration Experiments. We have previously estimated the R value of the dimeric protein by using DOSY experiments (Figure 2A). On the other hand, the C-Ring1B protein at 1.3 mM (where it would be mainly dimeric) eluted at 11.75 mL (Figure 2B). This elution volume yielded a R value of 21.9 ± 0.4 Å, which is similar to that obtained by the DOSY (22.8 ± 0.2 Å).

(b) Secondary Structure by FTIR Spectroscopy. FTIR is a powerful method for investigation of protein secondary structure. The main advantage in comparison with CD and fluorescence is that FTIR is much more sensitive to the presence of β-structure or random-coil and allows exploration of higher concentrations of protein (*45*). Structural information in proteins can be obtained by analyzing the amide I′ region of the spectrum (1700−1600 cm^{-1}). The absorbance of this band is mainly due to the stretching vibration of the carbonyl peptide bond, whose frequency is highly sensitive to hydrogen bonding and then to protein secondary structure (*46*).

The amide I′ band of C-Ring1B was centered near 1650 cm^{-1}. Band analysis decomposition showed components

Table 2: Secondary Structural Analysis of Dimeric C-Ring1B As Determined by FTIR[a]

wavenumber (cm^{-1})	structural assignment[b]	% of total secondary structure
1683	turns	7.3
1672	β-strands	5.1
1664	turns/3_{10} helix	6.0
1652	α-helix	46.8
1641	disordered structure	5.5
1629	β-strands	29.2

[a] Errors in the wavenumber are estimated to be ± 1 cm^{-1}. [b] There are two additional bands centered at 1604 and 1615 cm^{-1}. These bands are assigned to side chains and account for the 3% of the whole area of the amide I′ band. The percentages of secondary structure on the third column of the table do not take into account those bands. Band assignments have been carried out as described (*32*).

centered at 1683, 1672, 1664, 1652, 1641, 1629, 1615, and 1604 cm^{-1} (Table 2). The 1604 and 1615 cm^{-1} components correspond to side-chain vibrations, and the other maxima are assigned to vibration of groups involved in different secondary structural motifs (*45*): the 1629 cm^{-1} band is assigned to (π,0) β-sheet structure (*47*); the 1641 cm^{-1} band is assigned to random-coil structure (*48*); the 1652 cm^{-1} is assigned to α-helix (*49*, *50*); the 1672 cm^{-1} component is assigned to turns and loops (*46*) and also to the (0, π) β-sheet vibration band (*49*, *50*); the 1683 cm^{-1} band includes contributions from turns (*47*). In conclusion, the dimeric C-Ring1B was mainly composed of α-helix and β-sheet.

DISCUSSION

The Two-State Behavior of C-Ring1B. The self-organization of the native state of oligomeric proteins involves two steps: folding and association (*51*). The former is an unimolecular event, and the latter is a second-order event, since it involves the encounter of two or more molecules. The stability and the folding reaction of a number of small homodimeric proteins, such as Arc repressor (*52*), Trp aporepressor (*53*), human papilloma strain-16 E2 DNA binding domain (*54*), the C-terminal domain of the capsid of HIV (CAC) (*55*), and ORF6 (*56*), have been described in detail. All of them, except CAC, fold in the absence of detectable equilibrium intermediates in a coupled process that can be described as a two-state equilibrium. On the other hand, CAC folds *via* a monomeric intermediate, which maintains most of the structure observed when the monomer is forming the dimer (*55*).

In C-Ring1B, thermal denaturation experiments could not be carried out because of irreversibility. On the other hand, dimer dissociation followed by fluorescence and CD could not be observed, since in the explored concentration range (1−50 μM) the thermodynamical parameters were not concentration-dependent (Table 1, Figure 5B). This absence of protein-concentration dependence can be rationalized as follows.

First, both biophysical techniques could be spectroscopically silent to the dissociation step, because the structures (secondary and tertiary) of the dissociated monomers were similar to those of the monomers in the fully formed dimer. The similar environment for the fluorescence residues upon dimerization was confirmed by an additional piece of evidence. The NMR results at different concentrations showed the same set of up- or downfield shifted signals: (i) 2D-NOESY experiments carried out at 1 mM of protein concentration indicate that the chemical shift of the indole proton of the sole tryptophan residue appeared at 9.73 ppm (assigned on the basis of the strong NOEs with other protons of the indole ring); (ii) the 1D-DOSY experiments at concentrations below 5 μM showed a sharp singlet at the same chemical shift, suggesting that the environment of the indole proton did not change upon monomerization; (iii) the 1D-NMR spectrum of C-Ring1B at low concentrations (below 50 μM) showed upfield shifted methyl groups (data not shown) at −0.47, −0.30, 0.17, and 0.43 ppm, which remained unaltered when the protein concentration increased (up to 1 mM).

The second reason for the absence of the protein-concentration dependence in the $[GdmCl]_{1/2}$ value could rely on the fact that there was a small population of dimeric species at the protein concentrations used, which did not yield enough signal to be monitored by any technique. However, there was evidence of a protein-concentration dependence of the native baseline in CD, suggesting the presence of bimolecular event occurring below 1 M GdmCl (Figure 5B); unfortunately, protein concentrations higher than 60 μM could not be used in the spectropolarimeter because of the high voltage of the detector. Thus, although the CD and fluorescence agree in the obtained thermodynamical parameters for the monomeric protein, the presence of a probable dissociated monomeric state obscured by the native baseline in CD measurements indicates that the unfolding reaction of the dimeric C-Ring1B is not a two-state behavior. On the other hand, the fact that the two biophysical probes show agreement in the thermodynamical parameters for monomeric C-Ring1B suggests that unfolding of the monomeric protein is a two-state process (*57*).

The Stability of Monomeric C-Ring1B. Figure 6 shows the pH-dependence of ΔG of monomeric C-Ring1B at 298 K, obtained by fluorescence. The maximum conformational stability averages 5.2 ± 0.4 kcal mol^{-1} and occurred as a broad maximum between pH 6 and 8.5. The variation of ΔG with pH was greatest around pH 5, with a value of 1.2 kcal mol^{-1} **(**the difference between the ΔG at pH 6.0 and that at pH 5.0, Figure 6C**)**. At low pH, where native C-Ring1B was positively charged, the pK_as of the carboxyl groups in the folded protein are expected to be lower than in the unfolded protein because of buried residues (*58*). Thus, unfolded monomeric C-Ring1B binds protons more tightly than folded monomeric C-Ring1B, and this seems to be the main reason for the stability decrease of the protein as the pH was lowered. Similar behavior as the pH was varied has been observed in Ribonuclease A and Ribonuclease T (*59*, *60*), Barnase (*61*), the SAM (sterile alpha motif) domain of p73 (*62*), and staphylococcal nuclease (*63*−*65*).

The monomeric form of C-Ring1B is stabilized by 5.2 ± 0.4 kcal mol^{-1} relative to the denatured state, at pH 7. This value is at the lower end of the range determined for folded monomeric proteins (within the range 6 to 14 kcal mol^{-1}) (*38*). The free energy of dissociation of dimeric C-Ring1B, as obtained from the value of the dissociation constant (determined by the three techniques used in this work: 200 μM at 298 K), is 5.0 ± 0.4 kcal mol^{-1}. Thus, the energy of the unfolding of the monomeric species and the dissociation energy of the dimeric species are very similar. If we assume

than there are not significant structural changes upon dimerization (as suggested by the NMR results at different protein concentrations; see above), then the stability of the dimeric species relative to the denatured monomers would be ~15 kcal mol^{-1} (= 2 × 5.2 + 5.0) (at 1 M standard state), which is comparable to the values obtained for dimeric proteins of similar length (*66*). It seems that dimerization in C-Ring 1B is a rigid lock-and-key mechanism.

The pH-Induced Unfolding of Both Monomeric and Dimeric C-Ring1B Species. Since we have concluded that dimer dissociation is spectroscopically silent when using fluorescence (and probably CD), the pH-induced conformational changes observed by fluorescence and CD must be associated with the monomer. However, similar changes were observed by gel filtration, which monitors the dissociation of the dimeric species, as shown by the determination of the K_D (Figure 4B). Thus, it seems that the monomer and the dimer behaved similarly as the pH was modified. Conversely to that observed in other proteins (see, for instance, the work of Varadarajan and co-workers (*67*) and references therein), C-Ring1B does not dissociate at low pH (although we cannot rule out that the changes observed by gel filtration could be due to variations in the K_D). Since at low pH the charge of the protein increased, we must conclude that the charge of C-Ring1B did not play an important role in dimer formation/dissociation; rather, dimer formation/dissociation must be dominated by hydrophobic interactions between the subunits.

The average *m* value of monomeric C-Ring1B (2.7 kcal mol^{-1} M^{-1}) is large for a protein of its size (118-residues long), suggesting that the monomeric protein must bury a large surface upon folding (*68*). Moreover, the *m* value is pH-independent within the pH range where the protein was either folded or unfolded (Figure 6B). Whether or not the *m* value depends on pH differs from protein to protein. In Ribonuclease A, a linear relationship has been found (*59*), but a more complex behavior has been observed in Ribonuclease T1 (*59*), Barnase (*61*), the SAM domain of p73 (*62*), and staphylococcal nuclease (*64*, *65*). It has been suggested that a variation in the *m* value when pH decreases is related to the pK_a values of a putative conformational intermediate (*65*). Since the *m* value in C-Ring 1B is constant (Figure 6B), within the experimental error, it could be thought that no partially folded species could be populated at low pH. However, several pieces of evidence suggest the presence of a so-called molten-globule species at low pH (*69*, *70*): first, C-Ring1B at low pH contained a large amount of secondary structure (as shown by CD experiments, Figure 4A); second, these species at low pH must expose a large hydrophobic surface, as concluded from ANS binding experiments (Figure 3B); third, the fluorescence spectra indicate that most of the tertiary structure at low pH was disrupted (Figure 3A); finally, thermal- (Figure 1, Supporting Information) or chemical-denaturations (data not shown) did not show a sigmoidal behavior below pH 4. Thus, the lack of a pH-dependence in the *m* value does not imply the absence of an intermediate in monomeric C-Ring 1B.

The Biological Implications of the Presence of a Dimeric State of C-Ring1B. Protein self-association is a common phenomenon that can confer several structural and functional advantages to proteins, including improved stability, control over the accessibility and specificity of active sites, and increased complexity (*71*). Self-association restricts the presence of enzyme activity, in space, to specific sites within the cell. In some cases, as it happens in virus-encoded proteinases, self-association can restrict, in time, the infection stages. On the other hand, a mechanism preventing self-association through intramolecular interactions has been reported for some proteins. For instance, the WASP (Wiskott−Aldrich syndrome protein) family forms intramolecular interactions to hide regions involved in protein interactions (*72*); further, the cysteine proteinase of hepatitis A virus forms homodimers with a K_D in the milimollar range, which is decreased to 9 μM in the presence of viral RNA (*73*). Moreover, mutations that impair the self-association of spectrin (one of the major structural erythrocyte proteins) lead to clinically significant forms of hereditary elliptocytosis and pyropoikilocytosis (*74*). These examples show that self-association of proteins is physiologically important and thus imply that self-interacting protein complexes have abilities that monomers do not.

We have shown in this work that C-Ring1B is affected by a monomer−dimer equilibrium, and then probably the self-dimerization of Ring1B *via* its C-terminal domain can be used as a form of regulation. It could be thought, however, that the presence of such equilibrium would result from the used approach (i.e., working with protein fragments) and that the intact Ring1B would not dimerize. However, there are several pieces of evidence which suggest that the self-associating properties are intrinsic and specific to the entire polypeptide chain: (i) dimerization can be measured by three different techniques, which use different biophysical parameters (Figure 2); (ii) self-dimerization of C-Ring1B is highly specific by burying hydrophobic surfaces (ANS binding).

At effective concentrations, below 200 μM, Ring 1B would be mainly a monomer with a well-folded structure; this well-folded structure would be able to interact with the rest of the proteins of the PRC1 to regulate the *Hox* gene. The possibility of interacting with several proteins, in turn, would explain the ability of Ring1B to populate a well-folded and relatively stable monomer. The concentration of Ring1B *in vivo* is unknown and neither do we know whether the value of K_D measured here would be reduced in the presence of RYBP and M33, proteins which have been shown to interact with C-Ring1B (*16*, *17*), as it happens in the cysteine proteinase of hepatitis A virus upon binding to its partner biomolecule (*73*).

Conversely, if, by any reason, the concentration of Ring1B in the cell increased, then the protein would tend to dimerize. Dimerization could confer several structural and functional advantages to Ring1B: first, it would increase its stability (as shown by calculation of the free-energies); second, dimerization might probably hamper C-Ring1B interactions with Pc3, Ph2, and Bmi-1 proteins; finally, it would prevent oligomerization with other proteins, which could lead to pathogenic assemblies in the cell. In all this discussion, however, we have not considered the "crowding effect" present within the cell, which will affect the value of the K_D (*75*). At the present stage, it is necessary to carry out more experimental work to address how the self-dimerization of C-Ring1B would be affected by crowding agents. Also, more experiments are required to find out whether that dimerization would also abolish the interactions of C-Ring1B with RYBP and M33 or both. Further experiments will also be necessary

to elucidate whether Ring1A is also able to self-dimerize, or conversely, because of the shorter linker joining both conserved regions in Ring1B (Figure 1), whether self-dimerization is possible.

ACKNOWLEDGMENT

We thank an anonymous reviewer for his/her insights and helpful comments. We deeply thank May García, María del Carmen Fuster, and Javier Casanova for excellent technical assistance; we also thank Dr. German Rivas and Dr. Carlos Alfonso for performing the sedimentation equilibrium experiments in the early stages of this work. We thank Dr. M. Bycroft and Mr. M. Proctor for the kind gift of the histidine vector. We thank Sara Pozos for her involvement during the early stages of this work.

SUPPORTING INFORMATION AVAILABLE

A figure containing the thermal denaturations at different pHs of monomeric C-Ring1B followed by the changes in the ellipticity at 222 nm is available free of charge via the Internet at http://pubs.acs.org.

REFERENCES

1. Kentsis, A., and Borden, K. L. B. (2000) Physical mechanisms and biological significance of supramolecular protein self-assembly, *Curr. Protein Pept. Sci. 1*, 49−73.
2. Orlando, V. (2003) Polycomb, epigenomes and control of cell identity, *Cell 112*, 599−606.
3. Ringrose, L., and Paro, R. (2004) Epigenetic regulation of cellular memory by the Polycomb and Trithorax group proteins, *Annu. Rev. Genet. 38*, 413−443.
4. Francis, N. J., Saurin, A. J., Shao, Z., and Kingston, R. E. (2001) Reconstitution of a functional core polycomb repressive complex, *Mol. Cell 8*, 545−556.
5. Simon, J. A., and Tamkun, M. W. (2002) Programming off and on states in chromatin: mechanisms of Polycomb and trithorax group complexes, *Curr. Opin. Genet. Dev. 12*, 210−218.
6. Levine, S. S., Weiss, A., Erdjument-Bromage, H., Shao, Z., Tempsts, P., and Kingston, R. E. (2002) The core of the polycomb repressive complex is compositionally and functionally conserved in flies and humans, *Mol. Cell Biol. 22*, 6070−6078.
7. Cao, R., and Zhang, Y. (2004) The functions of E(Z)/EZH2-mediated methylation of lysine 27 in histone H3, *Curr. Opin. Genet. Dev. 14*, 155−164.
8. Gil, J., Bernard, D., and Peters, G. (2005) Role of polycomb group proteins in stem cell self-renewal and cancer, *DNA Cell Biol. 24*, 117−125.
9. Cao, R, Wang, L., Wang, H., Xia, L., Erdjument-Bromage, H., Tempst, P., Jones, R. S., and Zhang, Y. (2002) Role of histone H3 lysine 27 methylation in Polycomb-group silencing, *Science 298*, 1039−1043.
10. Muller, J., Hart, C. M., Francis, N. J., Vargas, M. L., Sengupta, A., Wild, B., Miller, E. L., O'Connor, M. B., Kingston, R. E., and Simon, J. A. (2002) Histone methyltransferase activity of a *Drosophila* polycomb group repressor complex, *Cell 111*, 197−208.
11. Francis, N. J., and Kingston, R. E. (2001) Mechanisms of transcriptional memory, *Nat. Rev. Mol. Cell Biol. 2*, 409−421.
12. Wang, H., Wang, L., Erdjument-Bromage, H., Vidal, M., Tempst, P., Jones, R. S., and Zhang, Y. (2004) Role of the histone H2A ubiquitination in polycomb silencing, *Nature 431*, 873−878.
13. de Napoles, M., Mermoud, J. E., Wakao, R., Tang, Y. A., Endoh, M., Appanah, R., Nesterova, T. B., Silva, J., Otte, A. P., Vidal, M., Koseki, H., and Brockdorff, N. (2004) Polycomb group proteins Ring1A/B link ubiquitynation of histone H2A to heritable gene silencing and X inactivation, *Dev. Cell 7*, 663−676.
14. Cao, R., Tsukada, Y. I., and Zhang, Y. (2005) Role of Bmi-1 and Ring1A in H2A ubiquitylation and Hox gene silencing, *Mol. Cell 20*, 845−854.
15. Wei, J., Zhai, L., Xu, J., and Wang, H. (2006) Role of Bmi1 in H2A ubiquitylation and hox gene silencing, *J. Biol. Chem. 281*, 22537−22544.
16. Schoorlemmer, J., Marco-Gutiérrez, C., Were, F., Martínez, R, García, E., Satjin, D. P. E., Otte, A. P., and Vidal, M. (1997) Ring1A is a transcriptional repressor that interacts with the Polycomb-M33 protein and is expressed at rhombomere boundaries in the mouse hindbrain, *EMBO J. 16*, 5930−5942.
17. García, E., Marcos-Gutiérrez, C., Lorente, M. M., Moreno, J. C., and Vidal, M. (1999) RYBP, a new repressor protein that interacts with components of the mammalian Polycomb complex and with the transcription factor YY1, *EMBO J. 18*, 3404−3418.
18. Li, Z., Cao, R., Wang, M., Myers, M. P., Zhang, Y., and Xu, R.-M. (2006) Structure of a Bmi-1-Ring1B group ubiquitin ligase complex, *J. Biol. Chem. 281*, 20643−20649.
19. Pace, C. N. (1986) Determination and analysis of urea and guanidine hydrochloride denaturation curves, *Methods Enzymol. 131*, 266−280.
20. Miroux, B., and Walker, J. E. (1996) Over-production of proteins in *Escherichia coli*: mutant hosts that allow synthesis of some membrane proteins and globular proteins at high levels, *J. Mol. Biol. 260*, 289−298.
21. Pace, C. N., and Scholtz, J. M. (1997) Measuring the conformational stability of a protein, in *Protein Structure* (Creighton, T. E., Ed.) 2nd ed., pp 253−259, Oxford University Press, Oxford.
22. Piotto, M., Saudek, V., and Sklenar, V. (1993) Gradient-tailored excitation for single-quantum NMR spectroscopy of aqueous solutions, *J. Biomol. NMR 2*, 661−665.
23. Price, W. S. (1997) Pulse-field gradient nuclear magnetic resonance as a tool for studying translational diffusion: Part I. Basic theory, *Concepts Magn. Reson. 9*, 299−336.
24. Price, W. S. (1998) Pulse-field gradient nuclear magnetic resonance as a tool for studying translational diffusion: Part II. Experimental aspects, *Concepts Magn. Reson. 10*, 197−237.
25. Lapham, J., Rife, J. P., Moore, J. P., and Crothers, D. M. (1997) Measurement of diffusion constants for nucleic acids by NMR, *J. Biomol. NMR 10*, 255−262.
26. Poveda, J. A., Fernández-Ballester, G., Prieto, M., and Neira, J. L. (2007) Dynamics of tryptophan in the histidine-containing phosphocarrier protein of *Streptomyces coelicolor*: evidence of multistate equilibrium unfolding, *Biochemistry 46*, 7252−7260.
27. Hinkle, A., Goranson, A., Butters, C. A., and Tobacman, L. S. (1999) Roles for the troponin tail domain in thin filament assembly and regulation. A deletional study of cardiac troponin T, *J. Biol. Chem. 274*, 7157−7164.
28. Álamo del, M., Neira, J. L., and Mateu, M. G. (2003) Thermodynamic dissection of a low affinity protein-protein interface involved in human immunodeficiency virus assembly, *J. Biol. Chem. 278*, 27923−27929.
29. Valdés, R., and Ackers, G. K., Jr. (1979) Study of protein subunit association equilibria by elution gel chromatography, *Methods Enzymol. 61*, 125−142.
30. Ackers, G. K. (1967) Molecular sieve studies of interacting protein systems. I. Equations for transport of associating systems, *J. Biol. Chem. 242*, 3026−3034.
31. Darlin, P. J., Holt, J. M., and Ackers, G. K. (2000) Coupled energetics of lambda cro repressor self-assembly and site-specific DNA operator binding I: analysis of cro dimerization from nanomolar to micromolar concentrations, *Biochemistry 39*, 11500−11507.
32. Muro-Pastor, M. I., Barrera, F. N., Reyes, J. C., Florencio, F. J., and Neira, J. L. (2003) The inactivating factor of glutamine synthetase, IF7, is a "natively unfolded" protein, *Protein Sci. 12*, 1443−1454.
33. Cooper, A., and Johnson, C. M. (1994) Isothermal titration calorimetry, *Methods Mol. Biol. 22*, 137−150.
34. Schmid, F. X. (1997) Optical spectrosocopy to characterize protein conformation and conformational changes, in *Protein Structure* (Creighton, T. E., Ed.) 2nd ed., pp 261−297, Oxford University Press, Oxford.
35. Royer, C. A. (1995) Fluorescence spectroscopy, in *Protein Stability and folding* (Shirley, B. A., Ed.) pp 65−89, Humana Press, Towota, NJ.
36. Echabe, I., Encinar, J. A., and Arrondo, J. L. R. (1997) Removal of spectral noise in the quantitation of protein structure through infrared band decomposition, *Biospectroscopy 3*, 469−475.
37. Cantor, C. R., and Schimmel, P. R. (1980), *Biophys. Chem.* W. H. Freeman, New York.

38. Creighton, T. E. (1993) *Proteins. Structures and macromolecular properties*. 2nd Ed., W. H. Freeman, New York.
39. Cavanagh, J. F., Wayne, J., Palmer, A. G., and Skelton, N. J., III. (1996) *Protein NMR spectroscopy: principles and practice*, Academic Press, San Diego, CA.
40. Thurlkill, R. L., Grimsley, G. R., Scholtz, J. M., and Pace, C. N. (2006) p*K* values of the ionizable groups of proteins, *Protein Sci. 15*, 1214−1218.
41. Semisotnov, G. V., Rodionova, N. A., Razgulyaev, O. I., Uversky, V. N., Gripas, A. F., and Gilmanshin, R. I. (1991) Study of the "molten globule" intermediate state in protein folding by a hydrophobic fluorescent probe, *Biopolymers 31*, 119−128.
42. Woody, R. W. (1995) Circular dichroism, *Methods Enzymol. 246*, 34−71.
43. Kelly, S. M., and Price, N. C. (2000) The use of circular dichroism in the investigation of protein structure and function, *Curr. Protein Pept. Sci. 1*, 349−384.
44. Hurtado-Gómez, E., Fernández-Ballester, G., Nothaft, H., Gómez, J., Titgemeyer, F., and Neira, J. L. (2006) Biophysical characterization of the Enzyme I of the *Streptomyces coelicolor* phosphoenolpyruvate:sugar phosphotransferase system, *Biophys. J. 90*, 4592−4604.
45. Arrondo, J. L. R., and Goñi, F. M. (1999) Structure and dynamics of membrane proteins as studied by infrared spectroscopy, *Prog. Biophys. Mol. Biol. 72*, 367−405.
46. Surewicz, W. K., and Mantsch, H. H. (1988) New insight into protein secondary structure from resolution-enhanced infrared spectra, *Biochim. Biophys. Acta 952*, 115−30.
47. Byler, D. M., and Susi, H. (1986) Examination of the secondary structure of proteins by deconvolved FTIR spectra, *Biopolymers 25*, 469−487.
48. Arrondo, J. L. R., Mantsch, H. H., Mullner, N., Pikula, S., and Martonosi, A. (1987) Infrared spectroscopic characterization of the structural changes connected with the E1−E2 transition in the Ca^{2+}-ATPase of sarcoplasmic reticulum, *J. Biol. Chem. 262*, 9037−9043.
49. Denning, D. P., Uversky, V., Patel, S. S., Fink, A. L., and Rexach, M. (2002) The *Saccharomyces cerevisiae* nucleoporin Nup2p is a natively unfolded protein, *J. Biol. Chem. 277*, 33447−33455.
50. Braiman, M. S., and Rothschild, K. J. (1988) Fourier transform infrared techniques for probing membrane protein structure, *Annu. Rev. Biophys. Biophys. Chem. 17*, 541−570.
51. Jaenicke, R., and Lille, H. (2000) Folding and association of oligomeric and multimeric proteins, *Adv. Protein Chem. 53*, 329−401.
52. Bowie, J. U., and Sauer, R. T. (1989) Equilibrium dissociation and unfolding of the Arc repressor dimmer, *Biochemistry 28*, 7139−7143.
53. Gittelman, M. S., and Matthews, C. R. (1990) Folding and stability of trp aporepressor from *Escherichia coli*, *Biochemistry 28*, 7139−7143.
54. Mok, Y. K., de Prat, Gay, G., Butler, P. J., and Bycroft, M. (1996) Equilibrium dissociation and unfolding of the dimeric papilloma virus strain-16 E2 DNA-binding domain, *Protein Sci. 5*, 310−319.
55. Mateu, M. G. (2002) Conformational stability of dimeric and monomeric forms of the C-terminal domain of human immunodeficiency virus-1 capsid protein, *J. Mol. Biol. 318*, 519−531.
56. Zeeb, M., Lipps, G., Lille, H., and Balbach, J. (2004) Folding and association of an extremely stable dimeric protein from *Sulfolobus islandicus*, *J. Mol. Biol. 336*, 227−240.
57. Jackson, S. E. (1998) How do small single-domain proteins fold, *Fold. Des. 3*, R81−R91.
58. Tandford, C. (1968) Protein denaturation, *Adv. Protein Chem. 23*, 121−282.
59. Pace, C. N., Laurents, D. V., and Thomson, J. A. (1990) pH dependence of the urea and guanidine hydrochloride denaturation of ribonuclease A and ribonuclease T1, *Biochemistry 29*, 2564−2572.
60. Yao, M., and Bolen, D. W. (1995) How valid are denaturant-induced unfolding free energy measurements? Level of conformance to common assumptions over an extended range of ribonuclease A stability, *Biochemistry 34*, 3771−3781.
61. Pace, C. N., Laurents, D. V., and Erickson, R. E. (1992) Urea denaturation of barnase: pH dependence and characterization of the unfolded state, *Biochemistry 31*, 2728−2734.
62. Barrera, F. N., Garzón, M. T., Gómez, F. J., and Neira, J. L. (2002) Equilibrium unfolding of the C-terminal SAM domain of p73, *Biochemistry 36*, 1129−1140.
63. Ionescu, R. M., and Eftink, M. R. (1997) Global analysis of the acid-induced and urea-induced unfolding of staphylococcal nuclease and two of its variants, *Biochemistry 36*, 1129−1140.
64. Whitten, S. T., and García-Moreno, E. B. (2000) pH dependence of stability of staphylococcal nuclease: evidence of substantial electrostatic interactions in the denatured state, *Biochemistry 39*, 14292−14304.
65. Whitten, S. T., Wooll, J. O., Razeghifard, R., García-Moreno, E. B., and Hilser, V. J. (2001) The origin of pH-dependent changes in *m*-values for the denaturant-induced unfolding of proteins, *J. Mol. Biol. 309*, 1165−1175.
66. Nett, K. E., and Timm, D. E. (1994) Conformational stability of dimeric proteins: quantitative studies by equilibrium denaturation, *Protein Sci. 3*, 2167−2174.
67. Bajaj, K., Chakshusmathi, G., Bachhawat-Sikder, K., Surolia, A., and Varadarajan, R. (2004) Thermodynamic characterization of monomeric and dimeric forms of CcdB (controller of cell division or death B protein), *Biochem. J. 380*, 409−417.
68. Myers, J. K., Pace, C. N., and Scholtz, J. M. (1995) Denaturant *m*-values and heat capacity changes: relation to changes in accessible surface areas of protein unfolding, *Protein Sci. 4*, 2138−2148.
69. Fink, A. L. (1995) Compact intermediate states in protein folding, *Annu. Rev. Biophys. Biomol. Struct. 24*, 495−522.
70. Ptitsyn, O. B. (1995) Molten globule and protein folding, *Adv. Protein Chem. 47*, 83−229.
71. Marianayagam, N. J., Sunde, M., and Matthews, J. M. (2004) The power of two: protein dimerization in biology, *Trends Biochem. Sci. 29*, 618−625.
72. Millard, T. H., Sharp, S. J., and Machensky, L. M. (2004) Signalling to actin assembly via the WASP (Wiskott-Aldrich syndrome protein) family proteins and the Arp2/3 complex, *Biochem. J. 380*, 1−17.
73. Peters, H., Kusov, Y. Y., Meyer, S., Bernie, A. J., Bauml, E., Wolff, M., Rademacher, C., Peters, T., and Grauss-Muller, V. (2005) Hepatitis A virus proteinase 3C binding to viral RNA: correlation with substrate binding and enzyme dimerization, *Biochem. J. 385*, 363−370.
74. Zhang, Z., Weed, S. A., Gallagher, P. G., and Morrow, J. S. (2001) Dynamic molecular modeling of pathogenic mutations in the spectrin self-association domain, *Blood 98*, 1645−1653.
75. Howlett, G. J., Minton, A. P., and Rivas, G. (2006) Analytical ultracentrifugation for the study of protein association and assembly, *Curr. Opin. Chem. Biol. 10*, 430−436.

BI701343Q